

Temperature induced deformations in BSO crystals due to photoconductivity

K. Leonhardt and H. J. Tiziani

Institut für Technische Optik
Universität Stuttgart*)

Prof. Dr. E. Menzel zum 65. Geburtstag gewidmet

Received 10 March 1983

Abstract

Deformations of $\text{Bi}_{12}\text{SiO}_{20}$ (BSO) crystals used in real-time metrology can lead to a degradation of the readout waves and of the diffraction efficiency. The deformations are due to heat, generated by the photocurrent under a transverse electric field. Thickness variations of the crystals and corresponding temperature changes on the crystal surfaces are measured as functions of the applied voltage and the electrical power, and intensity patterns due to the photoelastic effect are shown. Some precautions for operation of the crystal in practical applications are discussed.

Inhalt

Deformationen von BSO-Kristallen durch die Wärmewirkung des Photostromes. Deformationen durch Wärmedehnungen können in $\text{Bi}_{12}\text{SiO}_{20}$ (BSO)-Kristallen, die in der optischen Meßtechnik angewendet werden, zu Störungen in den Wellenfronten und zur Verringerung des Beugungswirkungsgrades führen. Die Wärmedehnungen entstehen durch den Photostrom des an den Kristall angelegten äußeren Feldes. Es werden Dickenänderungen und zugehörige Temperaturänderungen an der Kristalloberfläche als Funktion der angelegten Spannung und der elektrischen Leistung gemessen und Intensitätsmuster durch den spannungsoptischen Effekt gezeigt. Einige Konsequenzen für den praktischen Einsatz der Kristalle in Meßanwendungen werden besprochen.

1. Introduction

The application of photorefractive electrooptic crystals for real-time metrology is promising. Ferromagnetic materials such as Fe doped LiNbO_3 have been investigated extensively for optical storage. Recently, $\text{Bi}_{12}\text{SiO}_{20}$ (BSO) crystals have been used for holographic interferometry, speckle applications, contourline holography, optical correlation, phase conjugation, and

*) Pfaffenwaldring 9, 7000 Stuttgart 80.

vibration analysis (see e.g. [1–6]). They offer high sensitivity (100 to 300 $\mu\text{J}/\text{cm}^2$ at $\lambda \approx 500$ nm for a diffraction efficiency of 1 per cent) with good optical quality.

This paper reports on variations of crystal thickness and optical path length resulting from heat generation by photoconduction under the external electric field and thermally induced transient stresses. This dynamic effect which can degrade the interfering beams was not considered in early investigations of photoconductivity of BSO crystals [7, 8] and has been neglected in applications so far.

2. Mode of operation and a typical application of BSO crystals

For holographic interferometry and speckle applications the crystal is normally biased with a transverse electric field E_0 of 5 to 6 kV/cm (fig. 1) in order to enhance the diffraction efficiency [9, 10]. The physical process of forming the phase volume structure in the crystal can be described as follows: The crystal contains donors and trapping centres. Electrons are released under illumination with blue or green light into the conduction band (photoelectric effect). Under uniform illumination and with an external field applied the crystal acts as photoresistor. With spatially modulated light as in the case of holographic or speckle intensity structures, the electrons released in bright regions diffuse or drift into dark regions where they are trapped. This leads to a space charge field which modulates the refractive index through the electrooptic effect. Flooding with uniform illumination (or with the uniform reference beam) relaxes the space charge field and leads to an erasure of the stored information. For high intensity illumination > 10 mW/cm² the recording- and read-out-times are in the order of milliseconds (fig. 2). Holographic arrangements are shown in fig. 1. For holographic interferometry a memory tube or a video storage device facilitates the fringe pattern analysis. For the four-wave mixing arrangement (fig. 1 b) the transmitted part of the reference beam is used for reconstructing the real image after reflection at the mirror M. It can be extracted by the beamsplitter B S [11]. Since the crystals are optically active ($\rho \approx 45^\circ \text{mm}^{-1}$ at $\lambda = 514$ nm) different states of polarization for the diffracted image, zero order beam and scattered beam are observed [12], [13]. The polarizer in fig. 1 is used to separate the reconstructed wave from unwanted scatter noise beams or from the direct beam. A typical fringe pattern from a time averaged mechanical oscillation recorded on BSO is shown in fig. 3. No memory tube was required.

Fig. 4 shows the $(\bar{1}10)$ orientation of a cubic crystal of class 23 with its crystallographic axes x_1, x_2, x_3 , the unit cell of the lattice in relation to the axes of the optical set up x, y, z for a transverse electrooptic configuration with field direction $[110]$. Object beam and reference beam are in the x, z -plane. This results in a grating vector \vec{K} [14] in the x -direction. In this configuration the external field E_0 is transverse to the grating structure given by the holographic fringes of a plane wave object- and reference beam. Space charge grating and external field are in the same direction.

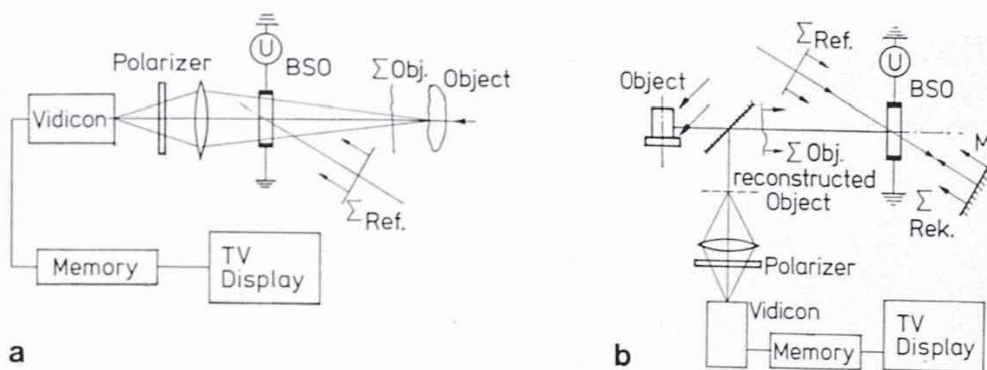


Fig. 1. a) Arrangement for holographic interferometry with the BSO-crystal in a transverse electrooptic configuration (two-wave mixing).

Σ_{Obj} = object wavefront

Σ_{Ref} = reference wavefront

b) Four-wave mixing configuration for holographic interferometry. Recording with Σ_{Obj} and Σ_{Ref} , reading out with the reference wave transmitted through the crystal and reflected back by the mirror M (Σ_{Rek}).

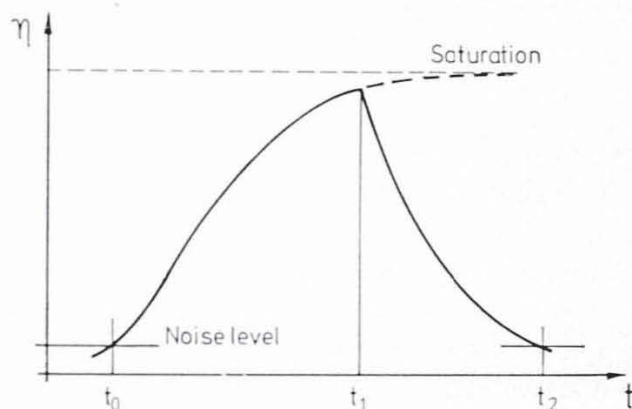


Fig. 2. Recording-erasure cycle for holography;

η = diffraction efficiency; t_0 to t_1 recording time; t_1 to t_2 read-out time.

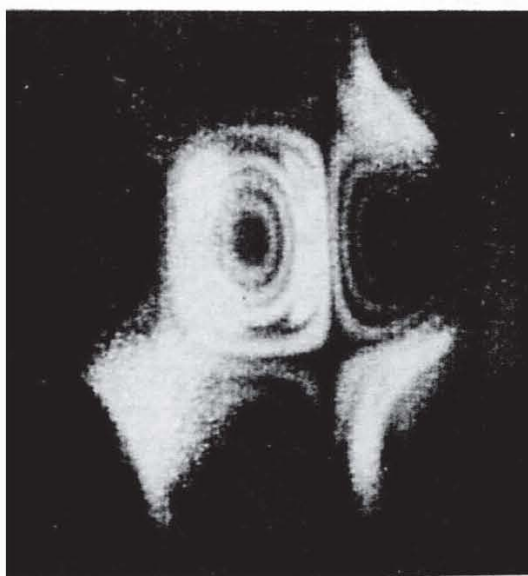


Fig. 3. Fringe pattern of a mechanical oscillation from a loudspeaker membrane recorded in time average with a BSO crystal. Higher order Bessel fringes can be seen.

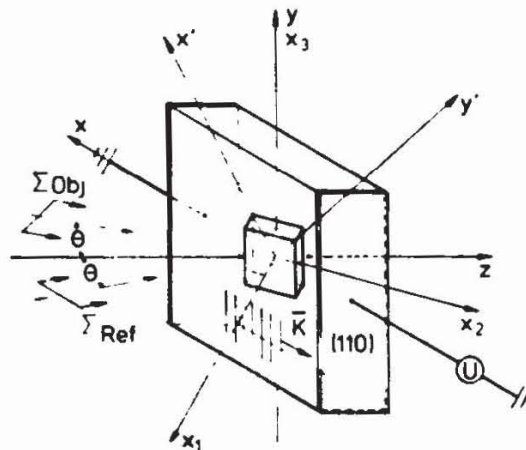


Fig. 4. Orientation of a crystal of class 23 cut in the $[\bar{1}10]$ direction under a transverse electric field E_0 in the $[110]$ direction; x_1, x_2, x_3 crystallographic axes; x, y, z axes of the optical setup.

Orientation of the phase volume grating due to plane object and reference beams in the x, z -plane; the incidence angles are θ and θ' and grating vector is \vec{K} in the $[110]$ direction.

For a plane wave propagating into the z -direction the crystal acts as non-linear wave plate with slightly elliptical characteristic waves. Their principal axes are in the x' and y' direction.

The crystal illuminated with uniform light under the external transverse electric field acts as photoresistor and is heated up by the photocurrent. In fact a superposed photocurrent is present in all practical applications. This photocurrent is not necessarily very small and can degrade the wavefronts and diffraction efficiency.

3. Experiments

Two BSO crystals from different manufacturers with different size and slightly different wavelength dependence of absorption were studied. Fig. 5

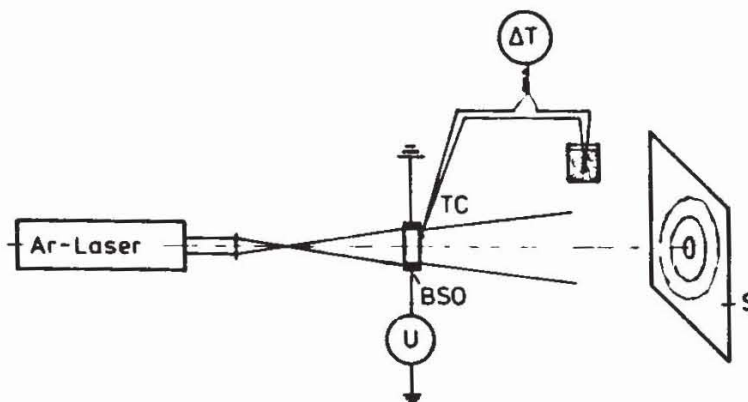


Fig. 5. Experimental arrangement for path difference and temperature measurement, S = observation plane, TC = thermocouple, U = Voltage for the external field.

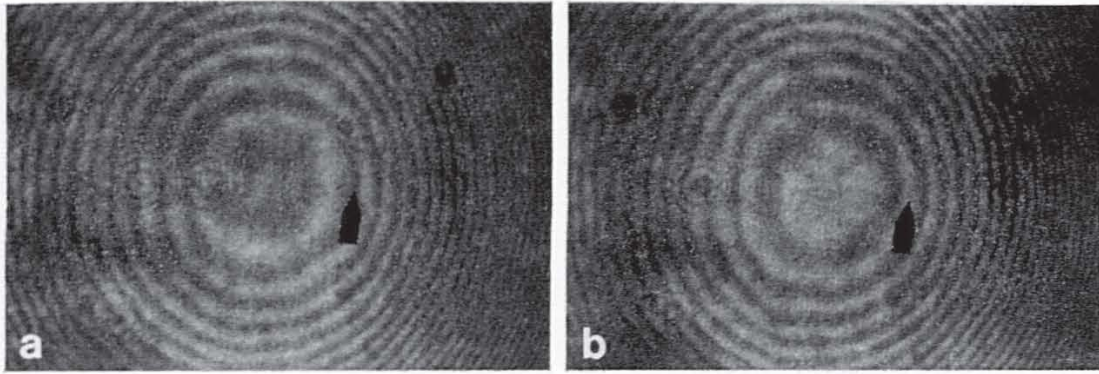


Fig. 6. Fringe displacement due to thickness variations of the crystal. Fig. 6a before switching on the voltage U ; Fig. 6b several seconds after switching on the voltage U

shows the experimental arrangement for temperature and pathlength difference measurement. The crystal is illuminated uniformly by an argon ion laser ($\lambda = 514 \text{ nm}$). By multiple reflections on the crystal faces interference fringes are obtained on the screen with good contrast due to the high refractive index ($n_{514} \approx 2,6$) of the crystals. Applying or increasing the electric field in the $[110]$ crystallographic direction (fig. 4) the fringes move from the center due to an increase of the crystal thickness as shown in fig. 6. The fringe movement is slow. The time from switching on the voltage until temperature equilibrium is reached is typically 7 seconds for $U = 3500 \text{ V}$ and $\Delta T \approx 8 \text{ K}$. The fringe movement can be reversed by switching off the applied voltage indicating a crystal contraction. The time constant is somewhat higher in this case.

In fig. 7 the number of additional fringes N_F is shown as a function of the voltage change U for two different levels of laser intensity I_1 and I_2 . The

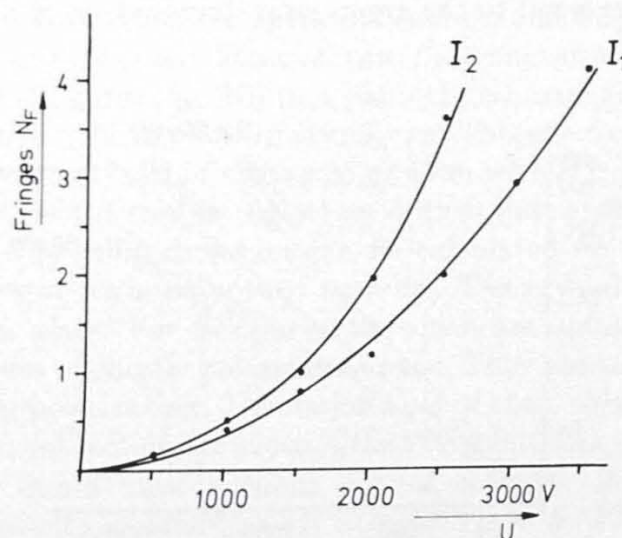


Fig. 7. Number of interference fringes N_F passing the mark in fig. 6 when switching on and off the electric field as a function of the voltage U for two mean intensity levels I_1 and I_2 on the crystal.

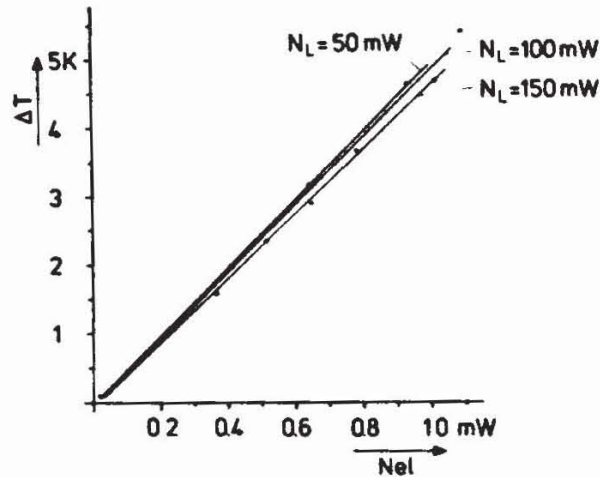


Fig. 8. Temperature change ΔT measured on the surface of the crystal with the thermocouple of fig. 5 as a function of the electrical power N_{el} of the photocurrent for three levels of laser output power.

functional dependence is seen to be quadratic which leads to a linear dependence on electrical power N_{el} .

$$N_F \propto \Delta T \propto N_{el} = \frac{U^2}{R}. \quad (1)$$

In (1) R is the resulting resistance of the crystal. Fig. 8 shows the temperature change ΔT as a function of N_{el} measured with a thermocouple fixed on the BSO-surface by a silver paste. The curves are linear with zero offset and nearly equal slope. They confirm the statement (1) by another independent measurement.

Fig. 9 shows the photocurrent measured by a galvanometer as a function of the voltage of the applied electric field. The different values of the photoresistance R correspond to the argon laser illumination of fig. 8, $R = f(I)$.

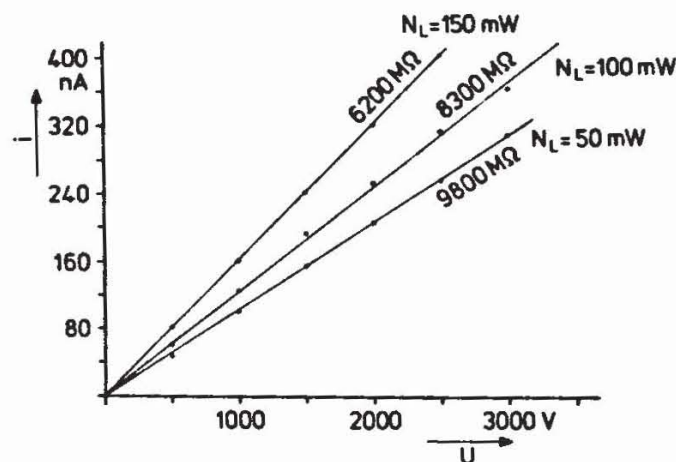


Fig. 9. Photocurrent i and photoresistance R as a function of the applied voltage U of the laser output power N_L .



Fig. 10. Transient interference figure in a photoelastic arrangement with converging beams on a crystal immediately after switching off the applied field. The interference figure is the fan-shaped dark region from the upper left to the lower right. In the lower half a dark region originates from a crack that occurred in the crystal. The dominant interference ring system results from interference between front and back surface as in fig. 6.

Applying the voltage without Ar laser illumination did not result in a measurable fringe movement and a significant temperature change on the crystal surface. In addition, no significant temperature change was observed by switching on and off the Ar laser illumination without electric field applied, indicating the photoresistance to be responsible for the crystal heating. For thicker crystals ($d = 2,4$ mm) from a different manufacturer a change of 12 fringes was measured together with a temperature change of 23 K.

In the transition time, where temperature changes and thickness variations of the crystal occur, thermal stresses can be demonstrated by transient crystal interference figures (fig. 10) in a photoelastic arrangement with converging beams and a polarizer acting as analyser. This effect can be explained as follows: In a cubic crystal of classes 23 or $\bar{4}3m$ with $[\bar{1}10]$ beam direction and $[110]$ electric field direction (fig. 4) an optical indicatrix [16] with axes perpendicular to the beam direction can be calculated for the equilibrium case of cubic crystal without optical activity. The crystal then acts as a linear retardation plate. For BSO crystals which are optically active, two characteristic waves of elliptic polarization exist. They are transmitted without any change in polarization. The major axes of their polarization ellipses for a plane wave in z -direction are those of the two principal axes a and b of the indicatrix which would exist without optical activity. In any case, for electrooptic coefficients as small as $r_{41} = r_{52} = r_{63} = 5 \cdot 10^{-10}$ [13] no intensity variations sufficiently large to produce visible crystal interference figures in this configuration can be obtained. If however thermal stresses occur during the transient time, the combined electrooptic and photoelastic

effect leads to interference figures of sufficient contrast during the transient time.

The figures appear with maximum contrast immediately after switching on and off the voltage and fade away with temperature equilibrium taking place.

4. Some aspects for practical measurements

For the applications of BSO crystals in contactless measuring procedures, abrupt variations of the electric field as well as of the light intensity of the waves at the crystal need to be avoided. Otherwise, the optical paths and hence the phases of the stored waves will be changed, and local intensity variations in the readout pattern will occur due to stress induced polarization changes in connection with the polarizers in fig. 1. The effect of smearing out the volume phase structure and the resulting loss in diffraction efficiency has not been investigated so far.

All these effects increase with the number of filled holes in the dark regions i.e. the influence is pronounced by working near or above exposure levels leading to crystal saturation. Some useful experimental procedures for successful work with BSO crystals were found to be:

1. uniform illumination over the whole surface to avoid inhomogeneities in the crystal temperature. Image plane holograms of discrete objects and Fourier plane holograms with strong zero orders are critical in this respect.
2. working with low mean intensity ($\lesssim 5 \text{ mW/cm}^2$) of the laser light on the crystal.
3. avoiding the interruption of the reference beam in the recording readout cycle of fig. 2 and in similar situations.
4. limiting the current for the external field ($i \lesssim 20 \mu\text{A}$). In addition, this avoids a crystal damage in the case of spark discharges.

We thank F. Höller and M. Küchel for their assistance and the DFG for the financial support.

References

- [1] Huignard, J.P., Phase Conjugation, Real-time Holography ... in Current Trends in Optics, edited by F.T. Arrechi and F.R. Aussenegg, Taylor & Francis, London (1981).
- [2] Huignard, J.P. and Herriau, J.P., *Appl. Optics* **16** (1977) 1807.
- [3] Tiziani, H.J., Leonhardt, K., Klenk, J., *Opt. Commun.* **34** (1980) 327.
- [4] Tiziani, H.J., *Optica Acta* **29** (1982) 463.
- [5] Yariv, Y., *Opt. Commun.* **25** (1978) 23.
- [6] Küchel, F.M., Tiziani, H.J., *Opt. Commun.* **38** (1981) 17.
- [7] Aldrich, R.E., Hou, S.L., Harvill, M.L., *J. Appl. Phys.* **42** (1971) 493.
- [8] Hou, S.L., Lauer, R.B., Aldrich, R.E., *J. Appl. Phys.* **44** (1973) 2652.
- [9] Huignard, J.P., Micheron, F., *Appl. Phys. Letters* **29** (1976) 591.
- [10] Peltier, M., Micheron, F., *J. Appl. Phys.* **48** (1977) 3683.
- [11] Huignard, J.P., Herriau, J.P., Valentin, T., *Appl. Optics* **16** (1977) 2796.
- [12] Herriau, J.P., Huignard, J.P., Aubourg, P., *Appl. Optics* **17** (1978) 1851.
- [13] Petrow, M.P. et al., *Optics Commun.* **31** (1979) 301.
- [14] Kogelnik, H., *Bell Syst. Techn. J.* **48** (1969) 2909.